



HAL
open science

Sunflower oil hydrogenation mechanisms and kinetics

Pierre Albrand, Carine Julcour-Lebigue, Florian Veyrine, Anne-Marie Billet

► **To cite this version:**

Pierre Albrand, Carine Julcour-Lebigue, Florian Veyrine, Anne-Marie Billet. Sunflower oil hydrogenation mechanisms and kinetics. *Chemical Engineering Journal*, 2021, 421 (1), 10.1016/j.cej.2021.129854 . hal-03219128

HAL Id: hal-03219128

<https://hal.science/hal-03219128>

Submitted on 6 May 2021

HAL is a multi-disciplinary open access archive for the deposit and dissemination of scientific research documents, whether they are published or not. The documents may come from teaching and research institutions in France or abroad, or from public or private research centers.

L'archive ouverte pluridisciplinaire **HAL**, est destinée au dépôt et à la diffusion de documents scientifiques de niveau recherche, publiés ou non, émanant des établissements d'enseignement et de recherche français ou étrangers, des laboratoires publics ou privés.



Open Archive Toulouse Archive Ouverte

OATAO is an open access repository that collects the work of Toulouse researchers and makes it freely available over the web where possible

This is an author's version published in: <http://oatao.univ-toulouse.fr/27774>

Official URL : <https://doi.org/10.1016/j.cej.2021.129854>

To cite this version:

Albrand, Pierre  and Julcour-Lebigue, Carine  and Veyrine, Florian and Billet, Anne-Marie  *Sunflower oil hydrogenation mechanisms and kinetics*. (2021) *Chemical Engineering Journal*, 421 (1). ISSN 1385-8947

Any correspondence concerning this service should be sent to the repository administrator: tech-oatao@listes-diff.inp-toulouse.fr

Sunflower oil hydrogenation mechanisms and kinetics

Pierre Albrand*, Carine Julcour, Florian Veyrine, Anne-Marie Billet*

Laboratoire de Génie Chimique, Université de Toulouse, CNRS, INPT, UPS, Toulouse, France

ARTICLE INFO

Keywords:
Hydrogenation
Isomerization
Vegetable oil
Mechanism
Kinetics

ABSTRACT

A kinetic model for sunflower oil hydrogenation on a palladium catalyst is proposed based on Horiuti–Polanyi type mechanism and considering either a dissociative or associative adsorption of hydrogen. The derived kinetic laws allow to explain the distinct dependency of saturation and isomerization reactions on hydrogen pressure.

Kinetic parameters are identified based on batch slurry hydrogenations carried out at 60–160°C and 2–31 bar with a powdered Pd/Al₂O₃ catalyst. A statistical analysis is used to select the most suitable adsorption mechanism for H₂. Evaluation of the Weisz–Prater modulus reveals that limitations to intraparticle diffusion occur despite the particle diameter does not exceed 40 μm.

1. Introduction

1.1. Context

The hydrogenation process traces back to late 19th century with Paul Sabatier and Jean-Baptiste Senderens [1] and is still a widely used process to reduce edible oils rancidity and increase their viscosity and melting point for food and cosmetics applications [2,3]. The objective is to saturate carbon–carbon double bonds (also known as *unsaturations*) in the presence of hydrogen and a supported metal catalyst as shown by the Eq. (1).



While double bonds are turned into single bonds (saturation reactions), isomerization reactions can also occur where *cis* unsaturations (hydrogen atoms are on the same side of the carbon chain) are turned into *trans* unsaturations (see Fig. 1). *Trans* fatty acids (TFA), and to some extent totally saturated fatty acids (SFA), can contribute to the development of cardiovascular diseases such as atherosclerosis [4,5]. As a consequence, the World Health Organization advises to reduce TFA and SFA consumption to a maximum of 1% and 10%, respectively, of the total caloric intake [6,7]. This urged public institutions to take action, as done by the European Union which demands less than 2 wt% of TFA in food products total fat content [8].

In this context, the hydrogenation process must focus on the partial saturation of polyunsaturated fatty acids (PUFA) while avoiding isomerization from *cis* to *trans* configuration. In other words, production of monounsaturated fatty acid (MUFA) with *cis* configuration must be favoured. In order to achieve such selectivity goals, kinetic rates and their dependency to operating conditions must be finely characterized as discussed in the following section.

1.2. Literature review

Two main factors affect edible oil hydrogenation selectivity: catalyst metal and operating conditions.

Concerning the metal, a compromise has to be reached between activity, selectivity and cost. Metals known to have the best selectivity towards MUFA are Rh, Pd, Pt, Ru, Ni in that decreasing order, while classification becomes Rh, Pd, Ru, Ni and Pt to enhance TFA production [9,10]. Hence, slurry of nickel based catalyst, which is mainly used at industrial scale, is rather chosen for its low cost than for its selectivity performances since the powder is often discarded after use [11]. Palladium catalyst is considered as a good compromise for *cis* MUFA selectivity [10], and has been applied in the form of structured catalysts in several studies [12–16].

Concerning operating conditions, their influences on selectivity are known: high temperatures tend to promote PUFA saturation and *cis* to *trans* isomerization, while high H₂ pressures limit the latter and boost all saturation reactions [17].

Kinetic models have been developed to consider, at least to some extent, this dependency to operating conditions. While some authors have used empirical laws to describe vegetable hydrogenation kinetics [18–20], others have based their models on reaction mechanisms.

Susu et al. [21] considered a Langmuir–Hinselwood type adsorption mechanism for palm oil hydrogenation over Ni catalyst. Fatty acids and H₂ have their own adsorption sites. Hydrogen adsorption is supposed to be dissociative and the two adsorbed hydrogen atoms (noted $\bar{\text{H}}$) are added simultaneously on unsaturations. Gut et al. [22] had an opposite approach where H₂ is supposed to be associative for sunflower hydrogenation with Ni based catalyst. Moreover, the two $\bar{\text{H}}$

* Corresponding authors.

E-mail addresses: pierre.albrand@toulouse-inp.fr (P. Albrand), annemarie.billet@toulouse-inp.fr (A.-M. Billet).

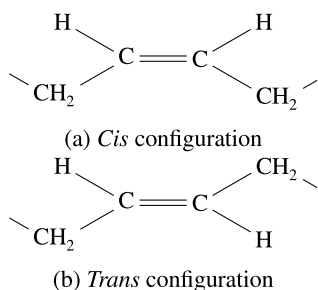


Fig. 1. Configurations of carbon-carbon double bonds (*unsaturations*) in unsaturated fatty acids.

are added to the ethylene bond in two steps following the so-called Horiuti-Polanyi reaction mechanism which allows to describe both saturation and isomerization reactions. The first added H gives an half-hydrogenated unsaturation which can be completely hydrogenated by the second H addition or conversely return to *cis* or *trans* unsaturation. Later on, Santacesaria et al. [23] and Fernández et al. [24] adopted this mechanism for rapeseed and sunflower oil hydrogenation over Pd catalysts, respectively. In both cases, saturation reactions dependency to operating conditions is well described. However, influence of the pressure on isomerization reaction is not considered which is not in agreement with experimental observations. To solve this shortcoming, Fillion et al. [25] used two distinct exponents for H₂ concentration in their isomerization kinetic laws (one for the *cis* to *trans* conversion, and another for the *trans* to *cis* conversion). Both parameters were optimized based on experimental data obtained during rapeseed oil hydrogenation. This empirical approach is not completely satisfactory because the model is only valid on a limited pressure range and the *trans/cis* thermodynamic equilibrium constant becomes a function of the hydrogen pressure, which is not in agreement with the van 't Hoff equation.

To study accurately the dependency of hydrogen pressure on the isomerization reactions, some authors did not consider the hydrogenation of edible oils (which are complex mixtures of triglycerides) but that of fatty acid methyl esters (FAME) instead. The advantages of the latter are the same reactivity as the fatty acid chains on triglycerides [26], but a higher effective diffusivity within the catalyst, hence avoiding internal mass transfer limitations [27]. In this context, Grau et al. [28] examined methyl oleate saturation and isomerization through an intermediate species, following once again the Horiuti-Polanyi reaction mechanism. By assuming a steady state approach for the absorbed species, a distinct reaction order for H₂ is noticed for the two reaction types. Jonker et al. [29] resumed this work and proposed twelve different kinetic laws depending on which reaction step is limiting. Nevertheless, the selected model did not consider the distinct dependency on hydrogen for the saturation and isomerization reactions. Deliy et al. [30] proposed a qualitative explanation of the hydrogenation of methyl linoleate into *cis* or *trans* methyl oleate which was taken over by Murzin and Simakova [31] later on: following the first addition of H on the methyl linoleate, the authors assumed the presence of either a pro-*cis* or pro-*trans* intermediate preceding the second addition of H and giving either the methyl oleate (*cis*) or the methyl elaidate (*trans*), respectively. Kinetic laws were derived but parameters values were not given.

From this state of the art, it can be concluded that (i) available kinetic models for edible oil hydrogenation do not consider a distinct dependency on hydrogen pressure for saturation and isomerization reactions, (ii) mechanisms were proposed for FAME hydrogenation to elucidate this effect, but their complexity prevented the optimization of associated kinetic parameters.

This work aims to propose a reaction mechanism for the sunflower oil hydrogenation that describes the hydrogen pressure effect on the

concomitant *cis/trans* isomerization. Sound hypotheses allow to simplify the derived reaction rate laws, in order to reduce the number of parameters. They are then optimized on an extensive range of operating conditions, based on hydrogenation assays carried out in a batch slurry reactor using Pd/Al₂O₃ catalyst. Confidence intervals for these parameters are finally discussed and a model is selected.

2. Reaction mechanism and kinetic laws

The presented mechanism is mainly inspired by the work of Grau et al. [28] who considered a half-hydrogenated intermediate during the hydrogenation of methyl oleate in agreement with the Horiuti-Polanyi mechanism. The current model goes further by considering the presence of PUFA and obeys the following assumptions:

- Sunflower oil is studied, hence the only considered fatty acids in triglycerides (TAG) are C18:2, C18:1 and C18:0.
- Because of high C18:2 reactivity, only C18:1 isomers are taken into account giving a total of four species: linoleic acid (C18:2 noted L), oleic acid (*cis* C18:1 noted C), elaidic acid (*trans* C18:1 noted T) and stearic acid (C18:0 noted S) [25].
- TAG and H₂ adsorb on distinct active sites noted ★ and *, respectively [21,23,24,28–31].
- TAG and H₂ adsorptions are supposed to be at equilibrium (not considered as limiting steps in the catalytic cycle) [28,29].
- H₂ adsorption is considered either associative or dissociative at first. [24,29]. The most suitable hydrogen adsorption mechanism is discussed later on.
- Stearic acid (S) does not adsorb on active sites [28].
- Surface coverage of intermediate species is neglected due to the high reactivity of these species [24].

2.1. Proposed reaction mechanism

Following the previous hypotheses, a first reaction scheme is derived whose mechanism is laid out in this section.

Hydrogen adsorptions at equilibrium are represented by Eq. (2) to (4) for the two mechanisms.

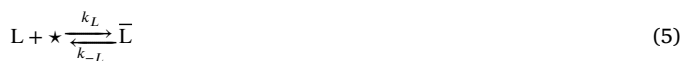
Dissociative adsorption:



Associative adsorption (second reaction at equilibrium):



Unsaturated fatty acids (L, C and T) adsorb on separate active sites:



Intermediate species containing one free unsaturation and one half-hydrogenated unsaturation ($\bar{\text{MH}}$) is obtained from the addition of an hydride ($\bar{\text{H}}$) on an absorbed linoleic acid, as shown by Eq. (8).



The free unsaturation either keeps its *cis* configuration or switches to a *trans* one [30,31]. The second H addition on the half-hydrogenated

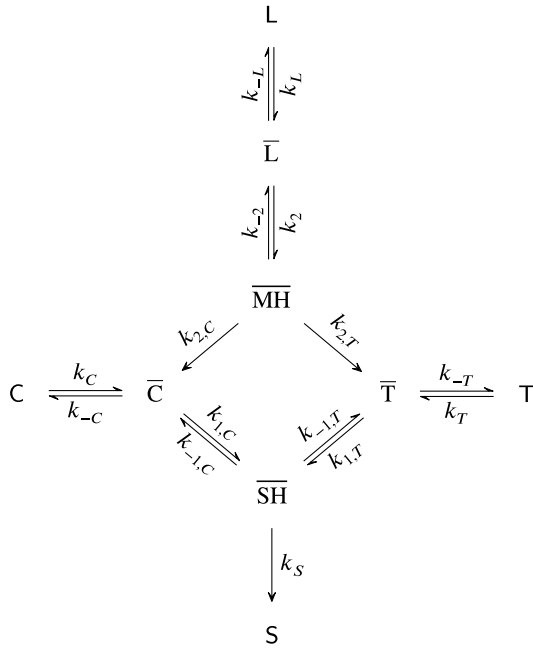


Fig. 2. Complete reaction scheme.

unsaturation is irreversible and gives either a *cis* or *trans* MUFA (see Eq. (9) and (10)).



In the same way, \overline{MH} intermediate is obtained, \overline{SH} intermediate comes from the addition of \bar{H} on either *cis* or *trans* adsorbed MUFA (see Eq. (11) and (12)). These surface reactions are reversible allowing *cis/trans* isomerization via \overline{SH} intermediate, as proposed by Grau et al. [28].



Finally, the second \bar{H} addition on \overline{SH} is irreversible. This gives a fully saturated fatty (S), which does not adsorb on $*$ sites, as shown by Eq. (13).



This mechanism can be summed up by Fig. 2.

2.2. Kinetic law derivation

Reaction rate expressions for the different species can be inferred from the previous mechanism. Furthermore, supplementary hypotheses allow to simplify the final model.

2.2.1. Initial expressions

First, overall formation rate of adsorbed species (\bar{L} , \overline{MH} , \bar{C} , \bar{T} , \overline{SH}) is set to zero [28]. Steady state approach is therefore assumed for these species, as shown from Eq. (14) to (18) where θ is the surface occupation of a given species.

$$\begin{aligned} r_{\bar{L}} &= k_L[L]\theta_* - k_{-L}\theta_L - k_2\theta_L\theta_H + k_{-2}\theta_{MH}\theta_* \\ &= -r_L - k_2\theta_L\theta_H + k_{-2}\theta_{MH}\theta_* = 0 \end{aligned} \quad (14)$$

$$r_{\bar{C}} = -r_C + k_{2,C}\theta_{MH}\theta_H - k_{1,C}\theta_C\theta_H + k_{-1,C}\theta_{SH}\theta_* = 0 \quad (15)$$

$$r_{\bar{T}} = -r_T + k_{2,T}\theta_{MH}\theta_H - k_{1,T}\theta_T\theta_H + k_{-1,T}\theta_{SH}\theta_* = 0 \quad (16)$$

$$r_{\overline{MH}} = k_2\theta_L\theta_H - k_{-2}\theta_{MH}\theta_* - k_{2,C}\theta_{MH}\theta_H - k_{2,T}\theta_{MH}\theta_H = 0 \quad (17)$$

$$r_{\overline{SH}} = k_{1,T}\theta_T\theta_H - k_{-1,T}\theta_{SH}\theta_* + k_{1,C}\theta_C\theta_H - k_{-1,C}\theta_{SH}\theta_* - k_S\theta_{SH}\theta_H = 0 \quad (18)$$

It is noticed that the consumption/production rates of unsaturated species in the liquid phase (r_L , r_C and r_T) appear in Eq. (14) to (16).

θ_{MH} and θ_{SH} expressions are deduced from Eq. (17) to (18) and a balance on hydrogen active sites ($\theta_H + \theta_* = 1$). They are available in Eq. (19) and (20).

$$\theta_{MH} = \frac{k_2\theta_L\theta_H}{k_{-2}(1-\theta_H) + (k_{2,C} + k_{2,T})\theta_H} = \frac{k_2\theta_L\theta_H}{\Delta_2} \quad (19)$$

$$\theta_{SH} = \frac{(k_{1,T}\theta_T + k_{1,C}\theta_C)\theta_H}{(k_{-1,T} + k_{-1,C})(1-\theta_H) + k_S\theta_H} = \frac{(k_{1,T}\theta_T + k_{1,C}\theta_C)\theta_H}{\Delta_1} \quad (20)$$

Reaction rates of liquid species, r_L , r_C and r_T are deduced from Eq. (14), (15) and (16), respectively, by introducing the expressions of θ_{MH} and θ_{SH} (see Eq. (19) and (20)). They are available from Eq. (21) to (23).

$$r_L = -\frac{k_2(k_{2,C} + k_{2,T})\theta_L\theta_H^2}{\Delta_2} \quad (21)$$

$$r_C = \frac{k_2k_{2,C}\theta_L\theta_H^2}{\Delta_2} + \frac{k_{-1,C}k_{1,T}\theta_T(1-\theta_H)\theta_H}{\Delta_1} - \frac{k_{-1,T}k_{1,C}\theta_C(1-\theta_H)\theta_H}{\Delta_1} - \frac{k_S k_{1,C}\theta_C\theta_H^2}{\Delta_1} \quad (22)$$

$$r_T = \frac{k_2k_{2,T}\theta_L\theta_H^2}{\Delta_2} - \frac{k_{-1,C}k_{1,T}\theta_T(1-\theta_H)\theta_H}{\Delta_1} + \frac{k_{-1,T}k_{1,C}\theta_C(1-\theta_H)\theta_H}{\Delta_1} - \frac{k_S k_{1,T}\theta_T\theta_H^2}{\Delta_1} \quad (23)$$

Hence, the production/consumption rates of fatty acids in the liquid phase are provided. However, active site coverage fractions for TAG and H_2 need to be expressed as a function of the operating parameters. For hydrogen, θ_H are given for dissociative and associative adsorption by Eq. (24) and (25), respectively, where $K_H = k_H/k_{-H}$.

Dissociative adsorption:

$$\theta_H = \frac{\sqrt{K_H C_{H_2}}}{1 + \sqrt{K_H C_{H_2}}} \quad (24)$$

Associative adsorption:

$$\theta_H = \frac{K_H C_{H_2}}{1 + K_H C_{H_2}} \quad (25)$$

As previously mentioned, coverage of active sites by intermediate species is assumed to be negligible compared to fatty acids. Hence, balance on vacant and occupied active sites $*$ gives Eq. (26).

$$\theta_L + \theta_C + \theta_T + \theta_* = 1 \quad (26)$$

Fatty acid adsorptions being at equilibrium, the fractional surface coverage θ_i for a given fatty acid i (standing for L, C or T) can be expressed as a function of the liquid phase concentration C_i , the equilibrium constant $K_i = k_i/k_{-i}$ and θ_* (see Eq. (27)).

$$\theta_i = K_i C_i \theta_* \quad (27)$$

Final θ_i expression is deduced from Eq. (26) and (27) and is given by Eq. (28).

$$\theta_i = \frac{K_i C_i}{1 + K_L C_L + K_C C_C + K_T C_T} \quad (28)$$

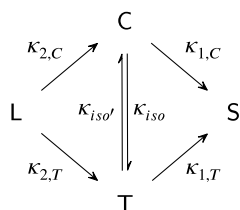


Fig. 3. Simplified reaction scheme.

2.2.2. Rate law simplification

Previous kinetic laws depend on numerous parameters which makes their identification difficult and possibly poorly accurate. Supplementary assumptions are made in order to simplify them.

First of all, \bar{H} first addition on \bar{L} is supposed to be irreversible, meaning that $k_{-2} \ll k_2$. Denominator Δ_2 in Eq. (19) is simplified:

$$\Delta_2 \approx (k_{2,C} + k_{2,T})\theta_H \quad (29)$$

In a similar way, $\bar{S}\bar{H}$ saturation is considered fast compared to its dehydrogenation. In other words, k_S is much higher than $k_{-1,T}$ and $k_{-1,C}$. Denominator Δ_1 in Eq. (20) is reduced to Eq. (30).

$$\Delta_1 \approx k_S\theta_H \quad (30)$$

Subsequently, Eq. (21) to (23) become Eq. (31) to (33).

$$r_L = -k_2\theta_L\theta_H \quad (31)$$

$$r_C = \frac{k_2k_{2,C}}{k_{2,C} + k_{2,T}}\theta_L\theta_H + \frac{k_{-1,C}k_{1,T}}{k_S}\theta_T(1 - \theta_H) - \frac{k_{-1,T}k_{1,C}}{k_S}\theta_C(1 - \theta_H) - k_{1,C}\theta_C\theta_H \quad (32)$$

$$r_T = \frac{k_2k_{2,T}}{k_{2,C} + k_{2,T}}\theta_L\theta_H - \frac{k_{-1,C}k_{1,T}}{k_S}\theta_T(1 - \theta_H) + \frac{k_{-1,T}k_{1,C}}{k_S}\theta_C(1 - \theta_H) - k_{1,T}\theta_T\theta_H \quad (33)$$

By introducing the overall constant κ_i , function of elementary constants k_i , Eq. (31) to (33) turn into Eq. (34) to (36). Production rate of S is deduced from a mass balance on all fatty acids, see Eq. (37).

$$r_L = -(\kappa_{2,C} + \kappa_{2,T})\theta_L\theta_H \quad (34)$$

$$r_C = \kappa_{2,C}\theta_L\theta_H + \kappa_{iso'}\theta_T(1 - \theta_H) - \kappa_{iso}\theta_C(1 - \theta_H) - \kappa_{1,C}\theta_C\theta_H \quad (35)$$

$$r_T = \kappa_{2,T}\theta_L\theta_H - \kappa_{iso'}\theta_T(1 - \theta_H) + \kappa_{iso}\theta_C(1 - \theta_H) - \kappa_{1,T}\theta_T\theta_H \quad (36)$$

$$r_S = \kappa_{1,C}\theta_C\theta_H + \kappa_{1,T}\theta_T\theta_H \quad (37)$$

Lumping several steps from the reaction scheme of Fig. 2 accordingly leads to Fig. 3.

Terms in Eq. (34) to (36) can be sorted out depending on whether they correspond to saturation reactions (associated to constants $\kappa_{2,C}$, $\kappa_{2,T}$, $\kappa_{1,C}$ or $\kappa_{1,T}$) or isomerization reactions (associated to constants κ_{iso} or $\kappa_{iso'}$). Then, it can be noticed that saturation reactions are proportional to θ_H and isomerization reactions to $(1 - \theta_H)$. Distinct dependency on hydrogen concentration is therefore obtained for the two reaction types. Saturation reactions are promoted by high θ_H (thus a high H_2 pressure) while isomerization ones are inhibited by such condition. This is in agreement with experimental observations.

This kinetic model gives a theoretical framework to describe the effect of operating conditions observed experimentally. Nonetheless, further simplifications are needed in order to gain robustness in parameter optimization (see Section 3.2).

Table 1

Sunflower oil composition before hydrogenation.

	Fatty acid	Molar fraction (-%)
	C14:0	0.07
	C16:0	5.93
<i>cis</i>	C16:1	0.09
<i>trans</i>	C16:1	–
	C17:0	0.04
<i>cis</i>	C17:1	–
	C18:0	3.83
<i>cis</i>	C18:1	29.92
<i>trans</i>	C18:1	0.01
<i>cis</i>	C18:2	58.54
<i>trans</i>	C18:2	0.02
<i>cis</i>	C18:3	0.12
<i>trans</i>	C18:3	0.06
	C20:0	0.27
<i>cis</i>	C20:1	0.14
<i>trans</i>	C20:1	–
	C22:0	0.73
<i>cis</i>	C22:1	–
<i>trans</i>	C22:1	–
	C24:0	0.24
<i>cis</i>	C24:1	–

3. Parametric identification

Previous section proposed theoretical kinetic laws for sunflower oil hydrogenation. From a practical stand point, parameters, which they depend on, have to be known either to quantify achievable selectivity or for continuous reactor sizing. Therefore, this section focuses on the determination of these parameters based on hydrogenation experiments.

3.1. Experimental data

3.1.1. Material & method

Refined sunflower oil was supplied by ITERG (Pessac, France) and its composition is given in Table 1.

Hydrogenations were carried out in a 100 mL autoclave (Parr Instrument). This reactor was equipped with an annular heating system and a cooling coil for temperature control. Upstream H_2 tank fed the dead-end reactor with constant pressure. A gas-inducing impeller insured efficient gas dispersion to remove gas–liquid mass transfer limitations.

For each experiment, 50 mL of oil and 15 mg of Pd/Al₂O₃ powdered catalyst (sieved between 20 and 40 μ m) were introduced inside the reactor. This catalyst was synthesized by Mecaprotec Industries (Muret, France) following a preliminary screening. Its active metal content is 0.7 wt%.

Once the reactor was sealed with the oil and catalyst inside, it was pre-heated at 2 bar under agitation speed of 200 RPM — well below critical speed for gas self-induction to prevent the starting of the reaction. When the desired temperature was reached, the reactor pressure was adjusted to match predefined operating conditions and the agitation speed was set at 1,400 RPM to initiate the reaction. Initial reaction rates were determined from recording pressure evolution in the upstream gas tank.

It must be mentioned that preliminary hydrogenation tests were carried out in the most favourable kinetic conditions (160°C - 31 bar) with different catalyst masses. Linear dependency between initial reaction rate and catalyst mass proved the reaction to operate without external mass transfer resistance.

Three to five samples of 2 mL were taken by experiment using a sampling line equipped with a filter. Analytic characterization of these samples was made by gas chromatography with flame ionization detection (GC/FID). They were methylated using boron trifluoride before being injected into an Agilent FAME column (0.25 mm ID \times 50 m,

Table 2

Available samples for the different sets of operating conditions (and number of separate experiments associated).

T (°C)	P (bar)			
	2	6	12.5	31
60	–	–	–	3 (1)
80	4 (1)	5 (1)	10 (2)	5 (1)
120	–	–	5 (1)	5 (1)
160	4 (1)	5 (1)	5 (1)	5 (1)

Agilent Select). The temperature settings for the oven were 165°C for 25 min, then 200°C for 13.5 min, and 250°C for 5 min. Helium was the carrier gas and its pressure was kept at 220 kPa with a split flow of 60 mL/min.

Positional isomerization also takes place during hydrogenation, resulting in the presence of numerous peaks on sample chromatographs. Identification of those peaks is precarious [32], hence they were lumped as *cis* or *trans* for C18:1 and C18:2. Conjugated PUFA (having one *cis* unsaturation and one *trans* unsaturation) were counted as *trans* C18:2.

3.1.2. Experimental data selection

Hydrogenation experiments were carried out with temperatures and pressures ranging from 60 to 160°C and from 2 to 31 bar, respectively. Experimental data set was first analysed with respect to the consistency of the measured initial reaction rates, which led to the exclusion of a few experiments: 12 were selected corresponding to 56 samples. Table 2 gives the distribution of these samples with respect to the operating conditions.

Out of the 21 fatty acids identified by GC, only 18-carbon fatty acid were considered since they contribute to about 90% of the weight. In agreement with the previously developed kinetic model, PUFA are considered as a whole (with no distinction between *cis* C18:2 and *trans* C18:2). Therefore, only the molar fractions of C18:2 (x_L), *cis* C18:1 (x_C), *trans* C18:1 (x_T) and C18:0 (x_S) are quantified for each sample.

In addition, it is possible to count the average number p' of remaining unsaturations per fatty acids for each sample. The saturation degree X is introduced by Eq. (38) where 0 subscript stands for the oil before hydrogenation.

$$X = \frac{p'_0 - p'}{p'_0} \quad (38)$$

3.2. Final kinetic model

Presented model in Section 2.2.2 went through further simplifications:

- κ_i constants follow Arrhenius type law,
- $\kappa_{2,C}$ and $\kappa_{2,T}$ ratio is supposed to be constant and is called ϕ ,
- $\kappa_{iso'}$ and κ_{iso} ratio is supposed to be constant and is called K_{iso} ,
- $\kappa_{1,C}$ and $\kappa_{1,T}$ are supposed to be equal and constant, and are called κ_1 .

The overall C18:2 saturation constant κ_2 is introduced as the sum of $\kappa_{2,C}$ and $\kappa_{2,T}$ (see Eq. (39)). Following the previous hypothesis, $\kappa_{2,C}$ over $\kappa_{2,T}$ ratio is given by Eq. (40).

$$\kappa_2 = \kappa_{2,C} + \kappa_{2,T} \quad (39)$$

$$\frac{\kappa_{2,C}}{\kappa_{2,T}} = \phi \quad (40)$$

Consequently, hydrogenation rates for PUFA hydrogenation into *cis* or *trans* MUFA are given by Eq. (41) and (42), respectively.

$$r_{2,C} = \frac{\phi}{1 + \phi} \kappa_2 \theta_L \theta_H \quad (41)$$

$$r_{2,T} = \frac{1}{1 + \phi} \kappa_2 \theta_L \theta_H \quad (42)$$

Additionally, SFA production rates from *cis* and *trans* MUFA are available Eq. (43) and (44), respectively.

$$r_{1,C} = \kappa_1 \theta_C \theta_H \quad (43)$$

$$r_{1,T} = \kappa_1 \theta_T \theta_H \quad (44)$$

Isomerization kinetic rates for *cis* to *trans* and for *trans* to *cis* MUFA are available Eq. (45) and (46), respectively.

$$r_{iso} = \kappa_{iso} \theta_C (1 - \theta_H) \quad (45)$$

$$r_{iso'} = \frac{\kappa_{iso}}{K_{iso}} \theta_T (1 - \theta_H) \quad (46)$$

The Arrhenius law equation for κ_i constants was reparametrized according to Eq. (47) to reduce correlation between the pre-exponential factor and the activation energy [33]. Reference temperature, T_{ref} , was set to 373 K.

Hydrogen adsorption constant, K_H , follows the van 't Hoff law, which was expressed using an analogous reparametrization.

$$\kappa_i = \kappa_{i,ref} e^{-\frac{E_{a_i}}{RT_{ref}} - \frac{T_{ref} - T}{T}} \quad (47)$$

Since there was no external mass transfer resistance, hydrogen concentration in the liquid is considered to be at its saturation value for the calculation of θ_H . This concentration at thermodynamic equilibrium is given by Eq. (48), where H_0 and ΔE are equal to 11.3 mol.m⁻³.bar⁻¹ and 5 kJ.mol⁻¹, respectively [25].

$$C_{H_2}^* = H_0 e^{-\frac{\Delta E}{RT}} P_{H_2} \quad (48)$$

Coverage fractions for unsaturated fatty acids, θ_i , were expressed in Eq. (28). In this section, it is assumed that MUFA have a unique adsorption constant, K_M , regardless of their *cis* or *trans* configuration [23,24]. Subsequently, $K_C = K_T = K_M$.

In addition, PUFA are supposed to have twice as many chances to adsorb than MUFA, hence $K_D = 2K_M$ [23,24].

Thus, the coverage fractions of the unsaturated fatty acids only depend on K_M and their concentrations in the liquid phase (see from Eq. (49) to (51)).

$$\theta_L = \frac{2K_M C_L}{1 + 2K_M C_L + K_M (C_C + C_T)} \quad (49)$$

$$\theta_C = \frac{K_M C_C}{1 + 2K_M C_L + K_M (C_C + C_T)} \quad (50)$$

$$\theta_T = \frac{K_M C_T}{1 + 2K_M C_L + K_M (C_C + C_T)} \quad (51)$$

Preliminary optimizations showed that K_M is large before 1, making unit term at the denominator negligible for θ_i . The numerical values of θ_i (and therefore the final results) being thus not sensitive to K_M , this parameter was arbitrarily set to 1 m³.mol⁻¹. Since the initial concentrations of unsaturated fatty acids are of an order of magnitude of 10³ mol.m⁻³, the unit term prevents the denominator to be close to zero only at high saturation level.

The final kinetic model parameters can be counted: three kinetic constants (κ_2 , κ_1 and κ_{iso}) and one adsorption constant (K_H). Four pre-exponential constants ($\kappa_{2,ref}$, $\kappa_{1,ref}$, $\kappa_{iso,ref}$ and $K_{H,ref}$), three activation energies (E_{a_2} , E_{a_1} and $E_{a_{iso}}$) and one heat of adsorption (E_H) must then be optimized. Two more constants have also to be added (ϕ and K_{iso}). Finally, **10 parameters** have to be identified for each hydrogen adsorption mechanism.

Table 3
Results for the first optimization step and comparison with values obtained by Fernández et al. [24].

	Dissociative		Associative		
	This work	Literature ^a	This work	Literature ^a	
$\kappa_{2,ref}$	17.26	0.47–2.03 ^b	4.58	0.119–0.442 ^{b,c}	kmol.s ⁻¹ .kg _{Pd} ⁻¹
E_{a_2}	20.82	34.9–58.2	24.38	48.9–58.2	kJ.mol ⁻¹
$\kappa_{1,ref}$	1.292	0.012–0.150 ^b	0.378	0.013–0.035 ^{b,c}	kmol.s ⁻¹ .kg _{Pd} ⁻¹
E_{a_1}	3.43	27.4–48.7	9.53	39.9–45.9	kJ.mol ⁻¹
$K_{H,ref}$	9.38×10 ⁻⁴	0.106–0.681 ^b	4.23×10 ⁻²	0.100–0.778 ^b	m ³ .mol ⁻¹
E_H	11.87	1.2–57.6	0.0411	5.8–8.3	kJ.mol ⁻¹
χ_1	1.36	–	1.18	–	

^aParameter range values obtained by Fernández et al. [24] for four dissociative parameter sets and four associative parameter sets.

^bReference temperature at 373 K in Fernández et al. [24] as well.

^cRecalculated since $\theta_H = K_H C_{H_2} / (2 + 2K_H C_{H_2})$ in Fernández et al. [24].

Table 4
Comparison of activation energy between this work and previous studies.

	Oil's type	E_{a_2} (J.mol ⁻¹)	E_{a_1} (J.mol ⁻¹)
This work (dissociative)	Sunflower	20,800	3,260
This work (associative)	Sunflower	24,400	9,530
Fernández et al. [24] (dissociative) ^a	Sunflower	48,800	40,500
Fernández et al. [24] (associative) ^a	Sunflower	51,700	46,400
Fillion et al. [25]	Soybean	72,999	50,151
Bern et al. [18]	Rapeseed	65,010	75,070
Snyder et al. [34]	Soybean	36,481	–
Gut et al. [22]	Sunflower	–	9,033
Chen et al. [19]	Soybean	78,454	30,837
Santacesaria et al. [23]	Rapeseed	12,500	14,700

^aAverage value of the parameter.



Fig. 4. Reactive scheme for the first optimization step.

3.3. Optimization strategy

The optimization requires the integration of mass balances to derive the time-concentration evolution of the unsaturated fatty acids. Moreover, the reaction rate expressions exhibit a non-linear dependency with respect to several kinetic parameters. To facilitate the parameters search, a two-step optimization is carried out as proposed by Fernández et al. [24].

A simplified kinetic model is first considered where no distinction between *cis* and *trans* MUFA is made. The overall MUFA concentration, C_M , is introduced as the sum of C_C and C_T ($\theta_M = \theta_C + \theta_T$). Only two reaction rates have to be accounted for: $r_2 = \kappa_2 \theta_L \theta_H$ and $r_1 = \kappa_1 \theta_M \theta_H$, as shown by Fig. 4.

Only the six parameters associated to κ_2 , κ_1 and K_H have to be identified first. Their optimization is based on a least-square method, where the χ_1 criterion estimates the sum of the mean quadratic errors between experimental fractions ($x_{L,exp}$ and $x_{M,exp}$) and corresponding model predictions ($x_{L,mod}$ and $x_{M,mod}$) for n_{sam} samples, as shown by Eq. (52).

$$\chi_1 = \sum_{i=1}^{n_{sam}} (x_{L,exp} - x_{L,mod})^2 + \sum_{i=1}^{n_{sam}} (x_{M,exp} - x_{M,mod})^2 \quad (52)$$

Once the first six parameters are identified, the second step considers the global reactive scheme of Fig. 3 to identify the last four parameters: ϕ , $\kappa_{iso,ref}$, $E_{a_{iso}}$ and K_{iso} .

Saturation degree, X , of most samples is inferior to 40%. In these conditions, *cis* and *trans* MUFA distribution is mainly affected by ϕ i.e. the PUFA tendency to get hydrogenated in a *cis* or a *trans* MUFA. Above 40% saturation degree, isomerization kinetic rates (r_{iso} and $r_{iso'}$) take over. For the second optimization, χ_2 criterion compares experimental and model x_T/x_C ratio (see Eq. (53)). This formulation gives

more weight to high *trans* content samples i.e. to highly hydrogenated samples. Subsequently, the criterion exhibits a greater sensitivity to $\kappa_{iso,ref}$, $E_{a_{iso}}$ and K_{iso} parameters value.

Moreover, while the first optimization step uses the species molar fractions at given reaction times, the second one considers values at given saturation levels. This eliminates potential bias induced by the first optimization step when the model does not perfectly fit the time-evolution of the experimental molar fractions.

$$\chi_2 = \sum_{i=1}^{n_{sam}} \left(\frac{x_{T,exp}}{x_{C,exp}} - \frac{x_{T,mod}}{x_{C,mod}} \right)^2 \quad (53)$$

Both optimization steps combine a stochastic and a deterministic approach in order to find a global minimum for χ_1 and χ_2 . For each optimization, the considered parameters are first initialized with values given by Fernández et al. [24]. A simulated annealing algorithm is first applied. Obtained values are then used as initialization for a Levenberg–Marquardt algorithm. This entire process is reiterated several times to insure that a minimum is found for both criteria.

MATLAB 2018b was chosen to achieve these optimizations.

3.4. Optimizations results

3.4.1. First optimization step

Identification of the first six parameters is carried out considering either dissociative or associative mechanism for hydrogen adsorption. Results are available in Table 3 and are compared to the ones from Fernández et al. [24].

χ_1 value is lower for the associative mechanism than for the dissociative one; however the difference is rather small and the later mechanism cannot be excluded at this stage (accounting for experimental errors).

First of all, it can be noted the heat of adsorption E_H tends to zero for associative mechanism, indicating thus a low dependency of K_H on temperature.

In addition, pre-exponential factors $\kappa_{2,ref}$ and $\kappa_{1,ref}$ are significantly higher in the dissociative case. Moreover, these reference constants at 373 K (see Eq. (47)) are 13 to 17 times higher than the ones from Fernández et al. [24] (see Table 3). This means that the Pd/Al₂O₃ catalyst used in this work is significantly more active.

As expected, E_{a_2} is superior to E_{a_1} for both mechanisms i.e. PUFA hydrogenation is favoured over MUFA hydrogenation at high temperatures, in agreement with experimental observations [17]. Fig. 5 shows the κ_2/κ_1 ratio as a function of temperature.

Nevertheless, the values E_{a_2} and E_{a_1} found in this work are both lower than 30 kJ.mol⁻¹ regardless of hydrogen adsorption mechanism. Comparison to previous studies confirmed that these activation energies are lower than expected (see Table 4), indicating probable internal mass transfer limitations.

Table 5
Results for the second optimization step and comparison with values obtained by Fernández et al. [24].

	Dissociative		Associative		
	This work	Literature ^a	This work	Literature ^a	
$\kappa_{iso,ref}$	1,010	237–623 ^b	1,283	89–266 ^b	$\text{kmol.s}^{-1}.\text{kPa}^{-1}$
Ea_{iso}	37.11	46.7–57.0	35.09	55.0–59.9	kJ.mol^{-1}
ϕ	4.49	-	2.44	-	-
K_{iso}	1.26	2	1.31	2	-
χ_2	0.503	-	0.654	-	-

^aParameter range values obtained by Fernández et al. [24] for four dissociative parameter sets and four associative parameter sets.

^bReference temperature at 373 K in Fernández et al. [24] as well.

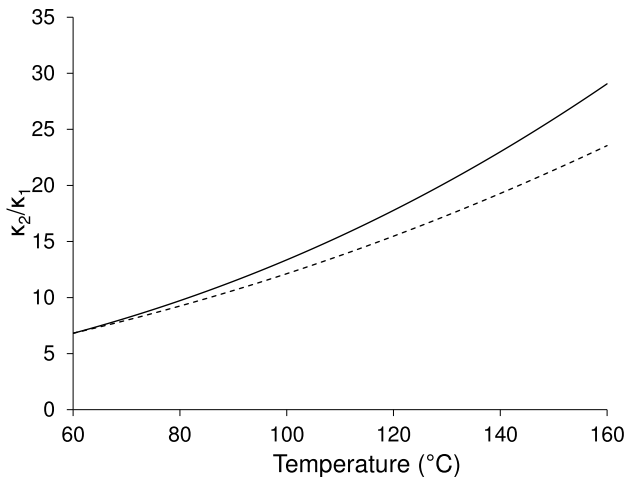


Fig. 5. κ_2/κ_1 ratio vs. temperature, for both H_2 adsorption mechanisms: dissociative (—) and associative (- -).

To quantify these mass transfer resistances, Weisz–Prater modulus, Ψ_{WP} , is calculated at the initial time of the reaction for H_2 and PUFA (L) as shown by Eq. (54).

$$\Psi_{WP} = \frac{n+1}{2} \frac{r_{app,i} (d_p/6)^2}{D_{eff,i} C_{S,i}} \quad (54)$$

$r_{app,i}$ is the apparent consumption rate of the reactant i and n is the corresponding apparent reaction order. If hydrogen is the limiting species then n varies between 0 and 0.5 for dissociative mechanism and up to 1 for the associative mechanism (see Eq. (24) and (25)). If L is limiting, n varies between 0 and 1 (see θ_L , Eq. (49)). Here the maximum values of n were applied. $C_{S,i}$ is the initial liquid phase concentration of the considered species. It is taken at saturation for a given temperature and pressure for H_2 , and initial concentration in the liquid phase for L. The particle diameter, d_p , is set at the mean value of 30 μm (see Section 3.1.1).

$D_{eff,i}$ is the effective diffusivity within the catalyst for the considered species i . It is calculated by Eq. (55) where $D_{i,oil}$ is either the H_2 or L (i.e. TAG) diffusivity in oil, ϵ_p and τ_p are the catalyst porosity and tortuosity, respectively. Expressions of $D_{i,oil}$ for both species in sunflower oil are available in Albrand et al. [35] for a given temperature. Porosity was measured at 75% for the same catalyst support [36] and tortuosity was set to 3 as an usual value [37].

$$D_{eff,i} = \frac{\epsilon_p D_{i,oil}}{\tau_p} \quad (55)$$

Fig. 6 gives the evolution of Ψ_{WP} for both mechanisms and both species over the investigated operating range (60–160°C, 2–31 bar). It

is recalled that the higher Ψ_{WP} value, the higher the internal mass transfer resistance. Ψ_{WP} values are above 0.1 meaning that diffusion within the catalyst is the limiting phenomenon. The limiting reactant depends on operating conditions: H_2 is more limiting at low pressure and high temperature, and vice versa for L.

The Weisz–Prater modulus of L is found to decrease with temperature, which is unusual. This behaviour can be explained by the high effect of the oil viscosity, μ_{oil} , on $D_{L,oil}$. Then, while κ_2 increases by a factor 5.7 and 7.6 for dissociative and associative mechanism, respectively, $D_{L,oil}$ is multiplied by a factor 10.6 on the same temperature range of 60–160°C.

Finally, the effectiveness factor can be deduced for r_2 in the least advantageous conditions. For $\Psi_{WP} > 3$, this factor is equal to $1/\Psi_{WP}$ [38], yielding a value of about 0.1.

3.4.2. Second optimization step

The values of the four last parameters are given in Table 5.

The χ_2 criterion is here lower for the dissociative mechanism, contrary to what was observed for χ_1 in the first optimization.

The parameter values are close for both mechanisms, except for ϕ . Activation energy Ea_{iso} values are significantly higher than Ea_2 and Ea_1 , meaning that r_{iso} and $r_{iso'}$ are particularly sensitive to temperature as compared to r_2 and r_1 (see Fig. 7). This also indicates that *cis* to *trans* isomerization is enhanced at high temperature, as expected [17]. Nevertheless, these values are still lower than the ones from Fernández et al. [24] (by 35%).

On the other hand, κ_{iso} constant at 373 K is up to 8 times higher, in agreement with the results obtained for $\kappa_{2,ref}$ and $\kappa_{1,ref}$ showing a high activity of the present catalyst.

ϕ value is above 1, meaning that PUFA is hydrogenated rather in *cis* than in *trans* MUFA. K_{iso} constant is also above 1, hence *trans* isomers are thermodynamically more stable than *cis* isomers, as expected.

Fig. 8 shows the time-evolution of fatty acid molar fractions for selected experiments and the respective model predictions calculated with the identified parameters. Although they do not allow to reproduce exactly all the experimental curves, the modelled reaction rates give a fair description of the effect of the operating conditions. Note that the differences between the two mechanisms are hardly noticeable.

The time-evolution of MUFA isomers is actually rather complex (see Fig. 8). First, fast PUFA hydrogenation gives mostly *cis* MUFA, with a maximum reached when PUFA fraction is close to 10%. Afterwards, isomerization reactions take over and *cis* isomer fraction drops. TFA fraction increases and exceeds the *cis* MUFA fraction. The ratio between the two MUFA fractions remains constant (reaching K_{iso}), and they decrease together to give SFA.

Fig. 9 gives the ratio between *trans* and *cis* MUFA as a function of the saturation degree. A plateau is reached at high saturation level for all models and is equal to K_{iso} . The lower the pressure and the higher the temperature, the lower the saturation degree at which this plateau is observed. This demonstrates a distinct dependency to temperature and pressure for saturation and isomerization reactions in the model. Finally, this figure shows a better agreement between modelled and experimental data when a dissociative adsorption of H_2 is assumed.

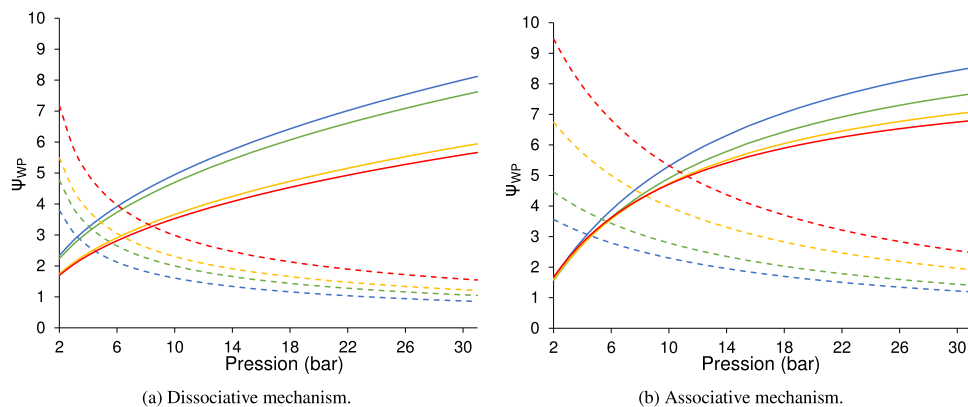


Fig. 6. Weisz-Prater modulus evaluation for H₂ (- -) and L/TAG (—) for both adsorption mechanisms: 60°C (blue), 80°C (green), 120°C (orange), 160°C (red).

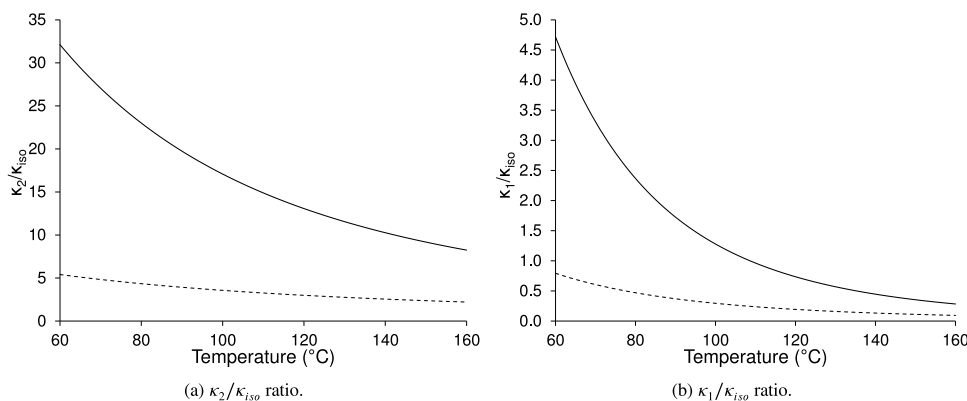


Fig. 7. κ_2/κ_{iso} and κ_1/κ_{iso} ratios vs. temperature for both H₂ adsorption mechanisms: dissociative (—) and associative (- -).

3.5. Confidence intervals of the parameters

In order to determine the confidence intervals for the previously identified parameters, the so-called *bootstrap* method was applied [39]. It consists in reproducing the optimization procedure (using previous values of the parameters as initialization) for a large number of different data sets generated from a random selection of the experimental samples: an overall number of 56 points is still considered, but some samples are over-represented while others are not included. By this way, a distribution of values is obtained for each identified parameter.

A total of 1,000 successive optimizations were carried out at each step. Results are represented in Fig. 10 showing the parameters mean values (close to previously obtained values) and their respective 95% confidence intervals. The latter are relatively small for the reaction rate constants at 373 K - $\kappa_{2,ref}$, $\kappa_{1,ref}$ and $\kappa_{iso,ref}$. On the other hand, confidence intervals for activation energies and heat of adsorption - Ea_2 , Ea_1 , Ea_{iso} and E_H -, are relatively narrow for the dissociative mechanism compared to the associative one.

This statistical analysis supports the previous conclusions that the H₂ adsorption mechanism best suited to describe the experimental data is the dissociative one.

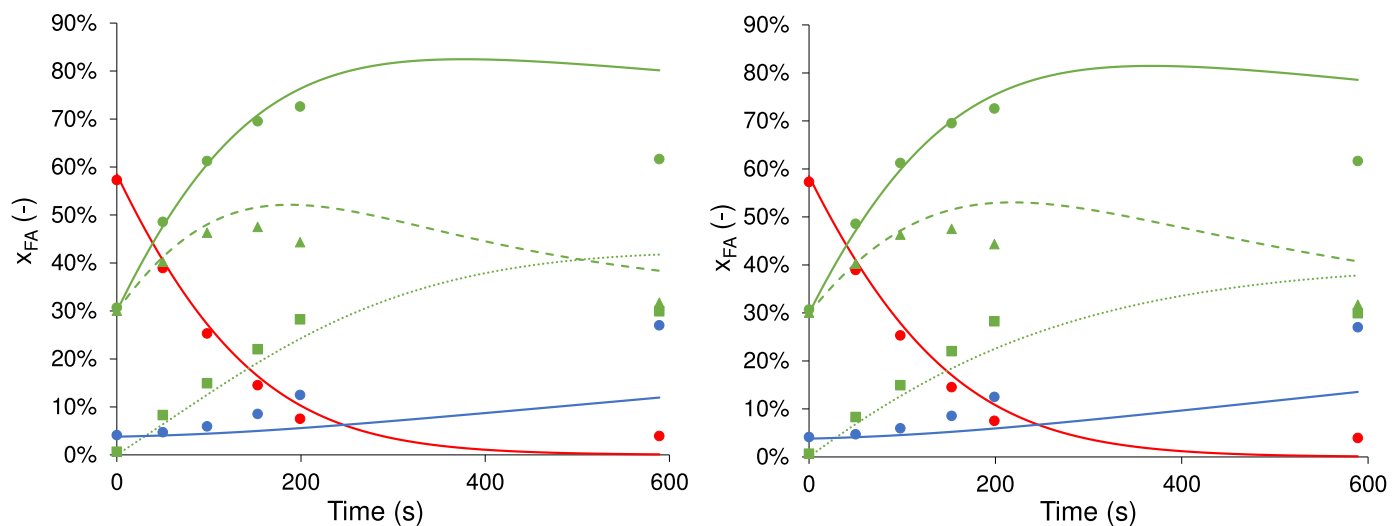
4. Conclusion

The main objective of this work was to propose a kinetic model for sunflower oil hydrogenation, able to consider the distinct trend

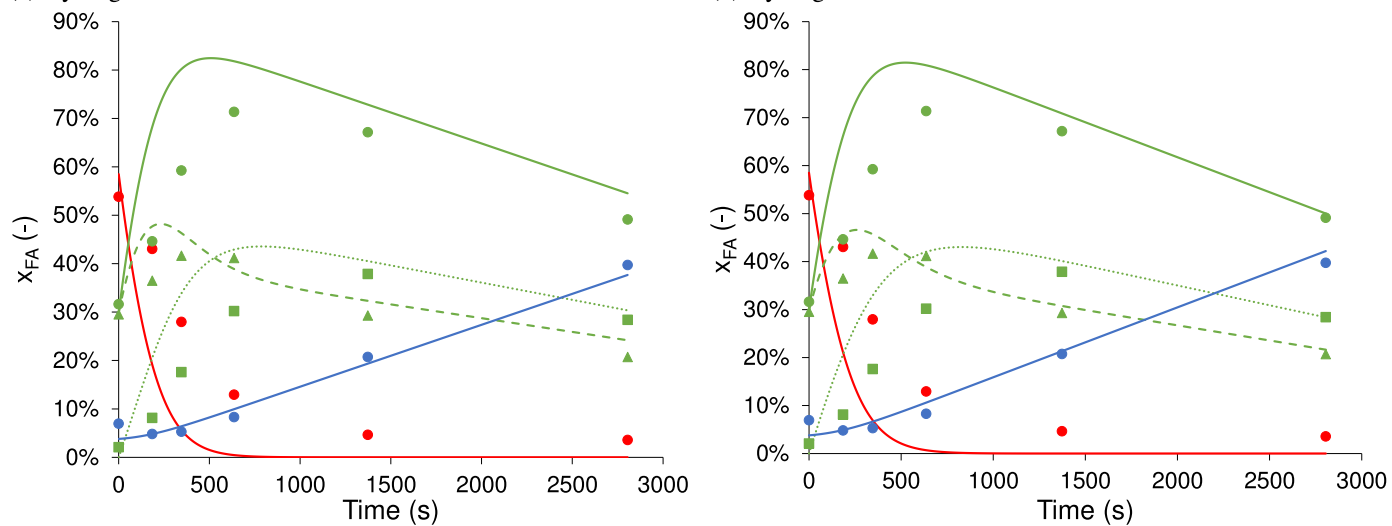
of saturation and isomerization reactions with respect to hydrogen pressure. To do so, the time-evolution of four fatty acid concentrations was monitored (C18:2, *cis* C18:1, *trans* C18:1 and C18:0). Horiuti-Polanyi mechanism was considered, assuming either a dissociative or an associative adsorption for H₂. In both cases, double bonds are either hydrogenated or isomerized through successive hydride additions. After simplifications, the deduced kinetic laws show that saturation and isomerization rates are proportional to θ_H and $(1 - \theta_H)$ respectively. As a consequence, high H₂ pressure enhances saturation reactions and reduces *cis/trans* isomerization.

A two-step optimization approach was applied to identify the corresponding kinetic parameters, based on deterministic and stochastic methods. The experimental data were obtained in the 2-31 bar and 60-160°C ranges, using a Pd/Al₂O₃ powdered catalyst.

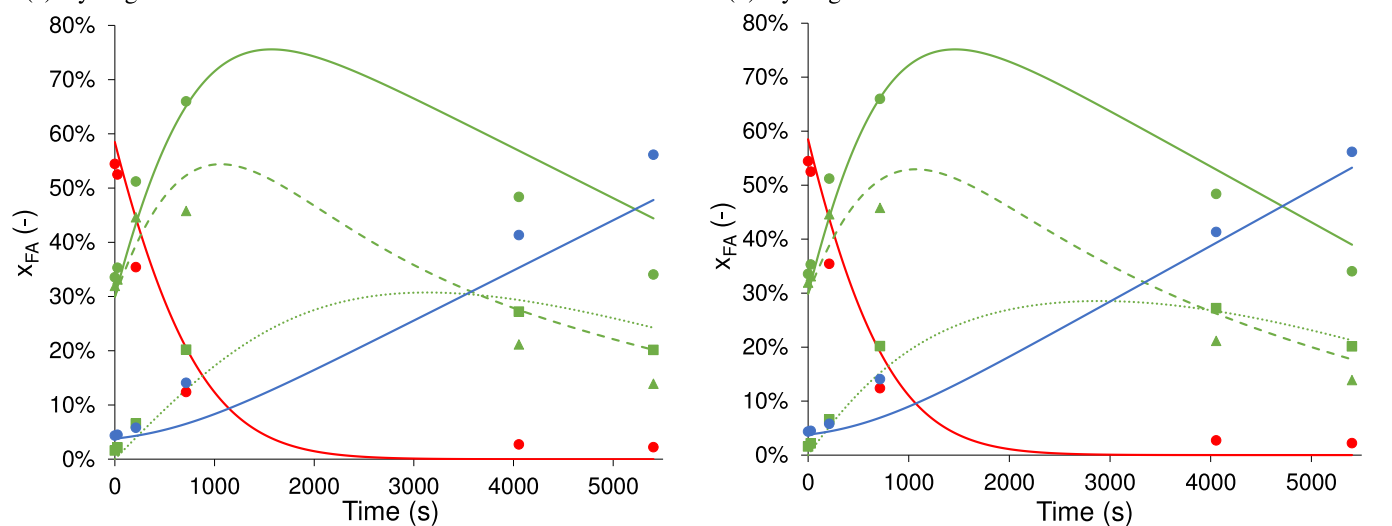
This catalyst being particularly active, significant internal mass transfer limitations were observed for both hydrogen and triglycerides despite the small mean diameter of the particles (30 μm). It resulted into rather low activation energies for the consecutive hydrogenation steps and an estimated effectiveness factor of about 0.1. Nonetheless, the isomerization reactions were found particularly sensitive to temperature. From the comparison of the ratio between *trans* and *cis* MUFA molar fractions and the calculation of the confidence intervals of the parameters, it was concluded that H₂ adsorption is most probably dissociative.



(a) Hydrogenation at 160°C - 12.5 bar for dissociative mechanism. (b) Hydrogenation at 160°C - 12.5 bar for associative mechanism.

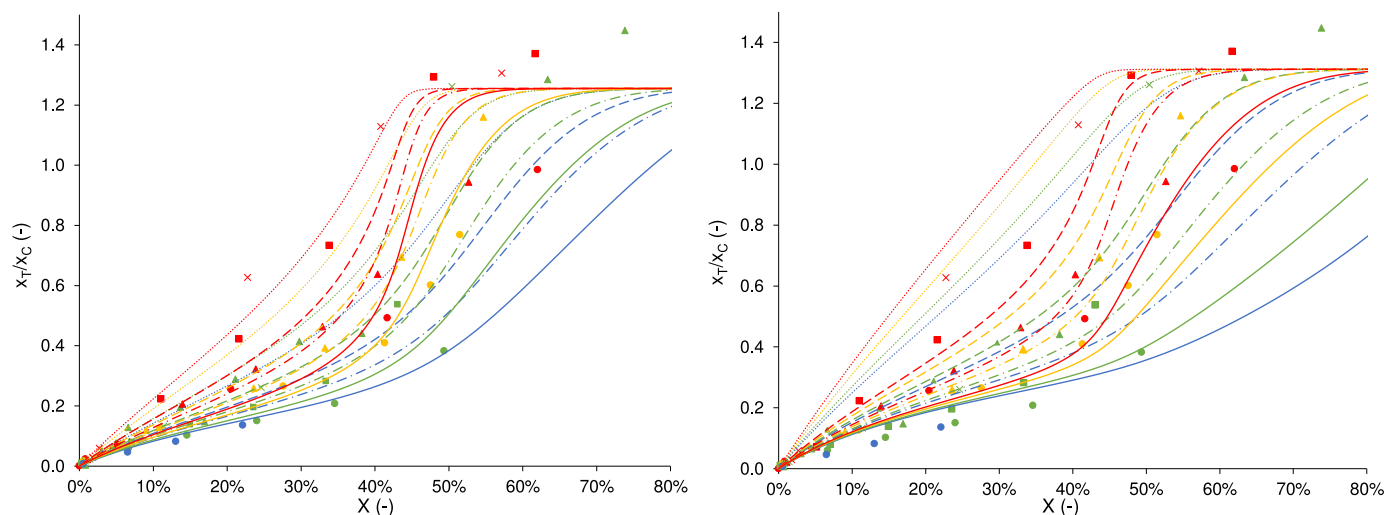


(c) Hydrogenation at 160°C - 6 bar for dissociative mechanism. (d) Hydrogenation at 160°C - 6 bar for associative mechanism.



(e) Hydrogenation at 80°C - 12.5 bar for dissociative mechanism. (f) Hydrogenation at 80°C - 12.5 bar for associative mechanism.

Fig. 8. Experimental data points and kinetic model curves for both H₂ adsorption mechanisms (dissociative left, associative right). C18:2 (red), C18:0 (blue), and C18:1 (green) compounds: overall (no *cis/trans* distinction) (●, —), *cis* (▲, - -), and *trans* (■, ...).



(a) Experimental data points and kinetic model for the dissociative mechanism. (b) Experimental data points and kinetic model for the associative mechanism.

Fig. 9. *Cis* C18:1 and *trans* C18:1 molar fractions ratio vs. saturation degree (X) for both H_2 adsorption mechanisms: 60°C (blue), 80°C (green), 120°C (orange), 160°C (red); 2 bar (X, ...), 6 bar (■, - -), 12.5 bar (▲, - · -), 31 bar (●, —).

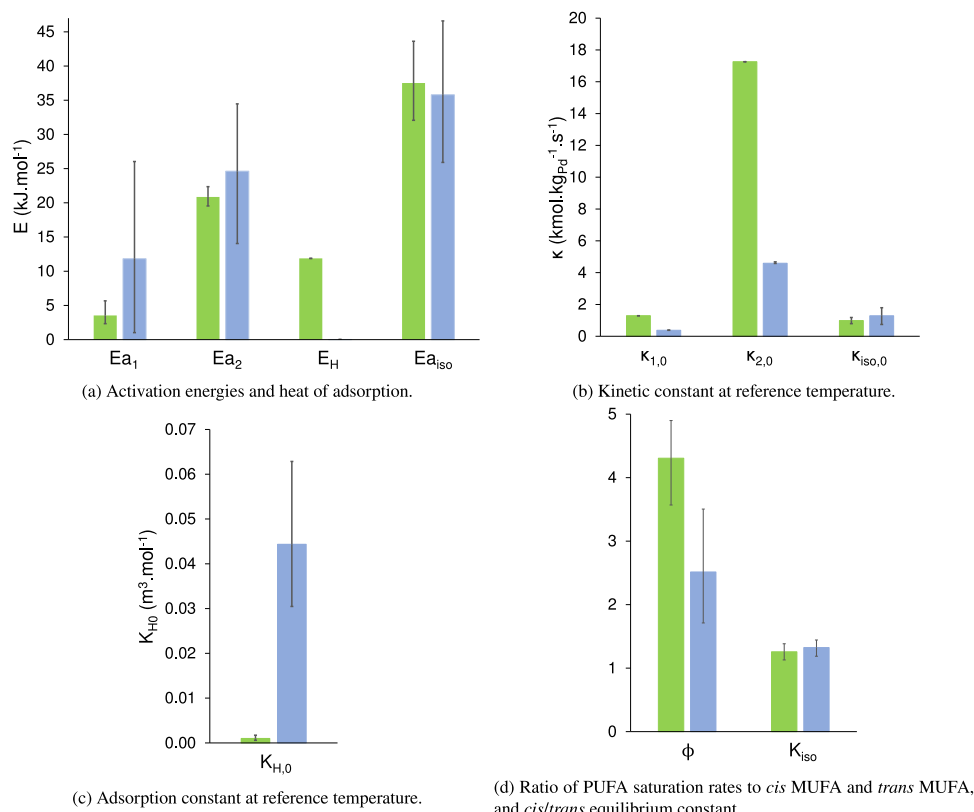


Fig. 10. Bootstrap results: average parameter values and confidence intervals at 95%; comparison between the dissociative (green) and associative (blue) mechanisms.

CRediT authorship contribution statement

Pierre Albrand: Conceptualization, Methodology, Software, Investigation, Model development and optimization, Data curation, Writing - original draft, Writing - review & editing. **Carine Julcour:** Funding acquisition, Methodology, Project administration, Supervision, Validation, Writing - review & editing. **Florian Veyrine:** Investigation, Data curation. **Anne-Marie Billet:** Funding acquisition, Methodology,

Project administration, Supervision, Validation, Writing - review & editing.

Declaration of competing interest

The authors declare that they have no known competing financial interests or personal relationships that could have appeared to influence the work reported in this paper.

Acknowledgements

This work was partly founded by Carnot-3BCAR Institute project entitled TOPACIS, in cooperation with *Institut des Corps Gras* (ITERG, Pessac, France) and *Laboratoire de Chimie Agro-industrielle* (LCA, Toulouse, France).

The authors wish to thank Guillaume Chollet from ITERG (Pessac, France) for his informative discussions concerning this work, Pierre Alphonse from CIRIMAT (Toulouse, France) and Mecaprotec Industries (Muret, France) for the catalyst development and synthesis.

References

- [1] P. Sabatier, J.-B. Senderens, Action du nickel sur l'éthylène. Synthèse de l'éthane, C. R. Acad. Sci. Paris 124 (1897) 1358–1360.
- [2] M. Kellens, G. Calliauw, Oil modification processes, in: *Edible Oil Processing*, second ed., John Wiley & Sons, Inc., 2013.
- [3] D.S. Cap, Cosmetic product including vegetable oil blend, 2014.
- [4] D. Mozaffarian, A. Aro, W.C. Willett, Health effects of trans-fatty acids: experimental and observational evidence, *Eur. J. Clin. Nutr.* 63 (S2) (2009) S5–S21.
- [5] R. Clarke, C. Frost, R. Collins, P. Appleby, R. Peto, Dietary lipids and blood cholesterol: quantitative meta-analysis of metabolic ward studies, *BMJ* 314 (7074) (1997) 112.
- [6] C. Nishida, R. Uauy, WHO Scientific update on health consequences of trans fatty acids: introduction, *Eur. J. Clin. Nutr.* 63 (S2) (2009) S1–S4.
- [7] R. Uauy, M. Gerber, P. Wolmarans, C.M. Skeaff, J.T. Brenna, M.A. Crawford, I. Elmadafa, C. Galli, Ghafoorunissa, C.J. Henry, A. Lapillonne, D. Li, D. Mozaffarian, W.M.N. Ratnayake, T. Sanders, A.J. Sinclair, *Fats and Fatty Acids in Human Nutrition*, Food and Agriculture Organization of the United Nations - FAO, 2011.
- [8] EU, Commission regulation (EU) 2019/649, 2019.
- [9] J.D. Ray, Behavior of hydrogenation catalysts. I. Hydrogenation of soybean oil with palladium, *J. Am. Oil Chem. Soc.* 62 (8) (1985) 1213–1217.
- [10] K. Belkacemi, A. Boulmerka, J. Arul, S. Hamoudi, Hydrogenation of vegetable oils with minimum trans and saturated fatty acid formation over a new generation of pd-catalyst, *Top. Catalysis* 37 (2) (2006) 113–120.
- [11] L. Faur, Transformation of fat for use in food products, in: *Oils & Fats Manual*, Lavoisier Publishing, 1992.
- [12] J.W. Veldsink, Selective hydrogenation of sunflower seed oil in a three-phase catalytic membrane reactor, *J. Am. Oil Chem. Soc.* 78 (5) (2001) 443–446.
- [13] A. Schmidt, R. Schomäcker, Partial hydrogenation of sunflower oil in a membrane reactor, *J. Mol. Catal. A Chem.* 271 (1) (2007) 192–199, URL: <http://www.sciencedirect.com/science/article/pii/S1381116907001513>.
- [14] M.-B. Macher, J. Hödberg, P. Møller, M. Härröd, Partial hydrogenation of fatty acid methyl esters at supercritical conditions, *Eur. J. Lipid Sci. Technol.* 101 (1999).
- [15] I.L. Simakova, O.A. Simakova, A.V. Romanenko, D.Y. Murzin, Hydrogenation of vegetable oils over Pd on nanocomposite carbon catalysts, *Ind. Eng. Chem. Res.* 47 (19) (2008) 7219–7225.
- [16] T. Boger, M.M. Zieverink, M.T. Kreutzer, F. Kapteijn, J.A. Moulijn, W.P. Addiego, Monolithic catalysts as an alternative to slurry systems: hydrogenation of edible oil, *Ind. Eng. Chem. Res.* 43 (10) (2004) 2337–2344.
- [17] J.W. Veldsink, M.J. Bouma, N.H. Schön, A.A. Beenackers, Heterogeneous hydrogenation of vegetable oils: a literature review, *Catal. Rev.* 39 (3) (1997) 253–318.
- [18] L. Bern, M. Hell, N.H. Schön, Kinetics of the hydrogenation of rapeseed oil: II. Rate equations of chemical reactions, *J. Am. Oil Chem. Soc.* 52 (10) (1975) 391–394.
- [19] A.H. Chen, D.D. McIntire, R.R. Allen, Modeling of reaction rate constants and selectivities in soybean oil hydrogenation, *J. Am. Oil Chem. Soc.* 58 (8) (1981) 816–818.
- [20] D. Krisnaiah, S. Sarkar, Kinetics of liquid phase hydrogenation of cottonseed oil with nickel catalysts, *J. Am. Oil Chem. Soc.* 67 (4) (1990) 233–238.
- [21] A.A. Susu, A.F. Ogunye, C.O. Onyegbado, Kinetics and mechanism of nickel-catalysed palm oil hydrogenation, *J. Appl. Chem. Biotechnol.* (1978) 823–833.
- [22] G. Gut, J. Kosinka, A. Prabucki, A. Schuerch, Kinetics of the liquid-phase hydrogenation and isomerisation of sunflower seed oil with nickel catalysts, *Chem. Eng. Sci.* 34 (8) (1979).
- [23] E. Santacesaria, P. Parrella, M. sm Di Serio, G. Borrelli, Role of mass transfer and kinetics in the hydrogenation of rapeseed oil on a supported palladium catalyst, *Appl. Catal. A Gen.* 116 (1) (1994) 269–294, URL: <http://www.sciencedirect.com/science/article/pii/0926860X94802947>.
- [24] M.B. Fernández, G.M. Tonetto, G. Crapiste, D.E. Damiani, Kinetics of the hydrogenation of sunflower oil over alumina supported palladium catalyst, *Int. J. Chem. React. Eng.* 5 (1) (2007).
- [25] B. Fillion, B.I. Morsi, K.R. Heier, R.M. Machado, Kinetics, gas-liquid mass transfer, and modeling of the soybean oil hydrogenation process, *Ind. Eng. Chem. Res.* 41 (4) (2002) 697–709.
- [26] P. van der Plant, J. van Oosten, Study of the mechanism of double-bond isomerization in methyl 9-octadecenoates, *J. Catal.* 38 (1–3) (1975) 223–230.
- [27] G.H. Jonker, J.W. Veldsink, A.A.C.M. Beenackers, Intraparticle diffusion limitations in the hydrogenation of monounsaturated edible oils and their fatty acid methyl esters, *Ind. Eng. Chem. Res.* 37 (12) (1998) 4646–4656.
- [28] R.J. Grau, A.E. Cassano, M.A. Baltanas, Kinetics of methyl oleate catalytic hydrogenation with quantitative evaluation of cis-trans isomerization equilibrium, *Ind. Eng. Chem. Process Des. Dev.* 25 (3) (1986) 722–728.
- [29] G.H. Jonker, J.-W. Veldsink, A.A.C.M. Beenackers, Intrinsic kinetics of 9-monoenoic fatty acid methyl ester hydrogenation over nickel-based catalysts, *Ind. Eng. Chem. Res.* 36 (5) (1997) 1567–1579.
- [30] I. Delyi, N. Maksimchuk, R. Psaro, N. Ravasio, V.D. Santo, S. Recchia, E. Paukshtis, A. Golovin, V. Semikolenov, Kinetic peculiarities of cis/trans methyl oleate formation during hydrogenation of methyl linoleate over Pd/MgO, *Appl. Catal. A Gen.* 279 (1–2) (2005) 99–107.
- [31] D.Y. Murzin, I.L. Simakova, Kinetic aspects of stereoselectivity in hydrogenation of fatty acids, *J. Mol. Catal. A Chem.* 286 (1–2) (2008) 156–161.
- [32] W.M.N. Ratnayake, G. Pelletier, Positional and geometrical isomers of linoleic acid in partially hydrogenated oils, *J. Am. Oil Chem. Soc.* 69 (2) (1992) 95–105.
- [33] M. Schwaab, L.P. Lemos, J.C. Pinto, Optimum reference temperature for reparameterization of the Arrhenius equation. Part 2: Problems involving multiple reparameterizations, *Chem. Eng. Sci.* 63 (11) (2008) 2895–2906.
- [34] J.M. Snyder, H.J. Dutton, C.R. Scholfield, Laboratory-scale continuous hydrogenation, *J. Am. Oil Chem. Soc.* 55 (4) (1978) 383–386.
- [35] P. Albrand, C. Julcour, V. Gerbaud, A.-M. Billet, Accurate hydrogenated vegetable oil viscosity predictions for monolith reactor simulations, *Chem. Eng. Sci.* 214 (2020) 115388.
- [36] F. Durán Martínez, Réacteur-échangeur de type monolith - stratégie de modélisation et description des phénomènes à l'échelle d'un canal catalytique unique (Ph.D. thesis), INP Toulouse, 2017, URL: <http://www.theses.fr/s175472>.
- [37] S. Kolitcheff, E. Jolimaitre, A. Hugon, J. Verstraete, P.-L. Carrette, M. Tayakout-Fayolle, Tortuosity of mesoporous alumina catalyst supports: Influence of the pore network organization, *Microporous Mesop. Mater.* 248 (2017) 91–98.
- [38] G.F. Froment, K.B. Bischoff, J.D. Wilde, *Chemical Reactor Analysis and Design*, Wiley, 2010, URL: https://www.ebook.de/de/product/12355179/gilbert_f_froment_kenneth_b_bischoff_juray_de_wilde_chemical_reactor_analysis_and_design.html.
- [39] B. Efron, Bootstrap methods: Another look at the Jackknife, 7 (1) (1979) 1–26, URL: <http://www.jstor.org/stable/2958830>.